Offshore wind energy potential in the era of climate change

Lucrezia Manservigi[a], Carlo Antonio Caputo[b], Pier Ruggero Spina[c] and Mauro Venturini[d]

[a] *University of Ferrara, Ferrara, Italy, lucrezia.manservigi@unife.it, CA*
[b] *University of Ferrara, Ferrara, Italy, carloantonio.caputo@unife.it*
[c] *University of Ferrara, Ferrara, Italy, pier.ruggero.spina@unife.it*
[d] *University of Ferrara, Ferrara, Italy, mauro.venturini@unife.it*

Abstract:

In the Net Zero Emissions Scenario, renewable sources — particularly wind energy — are expected to supply the majority of electrical power. Since the performance of wind turbines is strongly influenced by ambient conditions such as wind speed and air density, climate change may also alter wind energy production.
Thus, this study investigates how climate change could affect offshore wind energy production in Europe. The period 2000–2024 is adopted as the benchmark, while ambient conditions for 2050–2074 are projected under three scenarios defined by the Intergovernmental Panel on Climate Change, which assume different greenhouse gas concentration pathways.
The results indicate that the relative variation of offshore wind energy potential will be in the order of ±10 % compared to the benchmark period.

Keywords:

Wind Energy; Scenario Analysis; Energy Transition.

1. Introduction

Greenhouse gas (GHG) emissions produced by human activities are considered the main driver of climate change [1]. In response, several countries (e.g., EU) have set the ambitious goal to achieve net zero emissions by 2050, which can be met by significantly reducing the use of fossil fuels and increasing the role of renewable energies. Among renewable energy sources, wind energy is expected to be a key player to decarbonize the electricity sector [2]. However, the availability of wind energy, and consequently wind power, depends on ambient conditions (i.e., wind speed and air temperature) that have already changed due to climate change ([3], [4]). Thus, in-depth analyses are required to quantify the impact of climate change on wind energy, and its effect on wind power production.

Some studies have recently addressed this goal for offshore areas. Study [5] found that global offshore wind potential may experience a slight decline, particularly in Europe and China, with the exception of polar regions, where, on the contrary, an increase is projected. Studies [6] and [7] examined wind energy changes in Northern and Atlantic European waters. Study [6] reported an increase in wind energy density in the Baltic Sea of up to 10 %, while a widespread decrease was projected along the western coast of Ireland, with reductions up to 30 %. In contrast, study [7] projected a 10–15 % increase in wind energy across Atlantic European waters, particularly around Ireland and the UK. The impact of climate change in India's EEZ is more diversified, as projections vary depending on greenhouse gas concentration scenarios. Under the SSP2-4.5 scenario, a slight increase in wind resources is expected, whereas the SSP5-8.5 scenario forecasts a significant and widespread decline in the Arabian Sea and the Bay of Bengal [8]. In the Australian EEZ, offshore wind energy production is expected to decrease by 0.1–2.6 % over the next 50 years [9].

In summary, the state-of-the-art literature generally agrees on the following three key points.

First, on average, global offshore wind energy is going to decrease due to its migration from the mid-latitudes of the Northern Hemisphere to polar and tropical regions. As a consequence, the jet stream may become weaker, while stronger winds are expected near coastal areas due to the increase in sea-land temperature gradient [10]. On one hand, the decrease in wind power is dramatic since electricity production reduces, by challenging the pathway towards decarbonization. On the other hand, the decline in wind energy may also be

beneficial, since fewer ramp events are expected, by enhancing grid stability, reducing maintenance costs, extending the lifespan of wind turbines, and utilizing energy storage more effectively [11].

Second, climate change may influence the seasonal patterns of wind energy. For instance, in both the Atlantic Ocean and the Australian EEZ wind speed is projected to increase in summer, but may decrease in winter [6, 9]. Conversely, the period from September to December is expected to be windier in the Indian EEZ [8].

Third, wind energy is the renewable energy mostly affected by climate change, since it usually exhibits the highest variability with respect to hydro power and solar energy ([12], [13]).

Given the key role of wind energy in future decades, further studies are required to examine the impact of climate change. For instance, ambient conditions should be projected by means of different climate models and for different future scenarios, to either confirm or disconfirm the previous outcomes. In addition, most of the state-of-the-art literature mainly focuses on a few features (i.e., wind power density and average wind speed), but other variables (e.g., power output) should also be investigated. These findings can be used to (i) identify the most suitable areas for the installation of new wind turbines, and (ii) plan efficient policies that account for the influence of climate change [14].

This paper addresses these goals by evaluating the impact of climate change on offshore wind energy in Europe. To this purpose, we develop a methodology useful to assess wind energy density and power output over two different time frames (i.e., years 2000-2024 and 2050-2074 in this paper). We also analyze the distribution of wind speed over time, by evaluating the variation of its mean value, mode, scale factor, and shape factor. Three future scenarios, characterized by different representative concentration pathways (RCPs), namely RCP 2.6, RCP 4.5, and RCP 8.5, are analyzed.

The novelty of this study can be summarized as follows:

- analysis of the impact of climate change on multiple variables that characterize offshore wind energy;
- investigation of three RCP scenarios;
- high geographical (0.25° × 0.25°) and temporal (three hours) resolutions.

2. Methodology

This paper develops a general methodology aimed at assessing wind energy density (*WED*) of a given territory and the power generated by offshore wind turbines. To this purpose, two inputs are required: air temperature (*T*), and horizontal wind speed (*WS*). In addition, wind turbine characteristics (i.e., power curve, hub height *H*, rotor diameter *D*, and control strategy) have to be also known.
Air temperature and horizontal wind speed can be retrieved from the Copernicus Climate Data Store (CDS) [15], which provides data for the European domain split into cells (as shown in Fig. 1a) with a spatial resolution of 0.25° × 0.25° (approximately 28 km × 28 km).

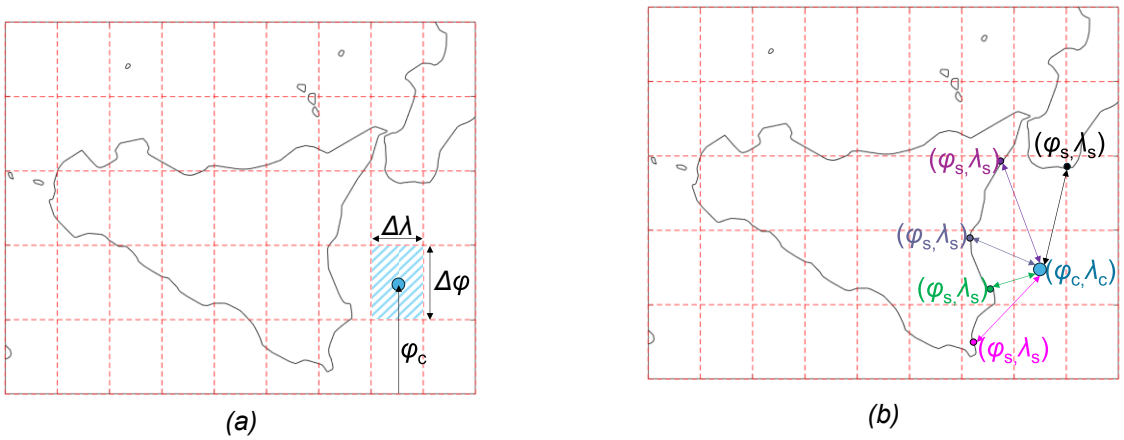

Figure 1. *Example of a) the split of a territory into cells, b) distance from the shoreline.*

In this database, wind speed values are reported at a height of 10 m above ground level, whereas air temperature *T* (expressed in °C) refers to a measurement height of 2 m. To obtain the corresponding values at the turbine hub height (*H*), Eqs. (1)-(3) are applied ([16], [17]). Hellman exponent (α) depends on hub height (*H*) as well as on surface roughness (*z*) that is set equal to 0.0002 m for offshore areas [17]. In Eq. (3), the parameter γ is the atmospheric temperature lapse rate, which describes the decrease in temperature with altitude, and is assumed to be 0.0065 °C/m [18].

$$WS_H = WS_{10\,m} \cdot \left(\frac{H}{10}\right)^{\alpha} \quad (1)$$

$$\alpha = \frac{1}{\ln\left(\frac{H}{z}\right)} \quad (2)$$

$$T_H = T_{2\,m} - (H - 2)\cdot\gamma \quad (3)$$

Air pressure at hub height (p_H) is calculated as in Eq. (4), where g is the gravitational acceleration, and R is the gas constant for air (i.e., 287.04 J/kg·K).

$$p_H = 101{,}325\cdot\left[1 - \frac{\gamma\cdot(H - 2)}{T_H + 273.15}\right]^{\frac{g}{R\cdot\gamma}} \quad (4)$$

Air density (ρ) can be estimated as in Eq. (5).

$$\rho_H = \frac{p_H}{R\cdot[T_H + 273.15]} \quad (5)$$

The yearly wind energy density *WED* (Eq. (6)) assesses wind potential per unit of rotor swept area over a given time frame. If N years are considered, the contribution of N_t time stamps has to be accounted for with time granularity Δt.
Instead, power output P_{WT} is proportional to the number of wind turbines (N_{WT}) that can be installed within a given cell. This value depends on the area that can effectively be exploited for wind turbine installation (A_{WT} in Eq. (7)), which depends on the availability factor a_f. The availability factor represents the maximum fraction of a given cell area A_{cell} that is available for wind turbine deployment [19]. The value of a_f depends on the distance from the shore (d) [19], which can be evaluated by using Eqs. (8) – (10). Specifically, θ denotes the central angle between two points on a sphere. For each offshore cell, θ is computed by means of the haversine formulation (Eq. (10)), where φ_c and λ_c are latitude and longitude, respectively, of a given cell centroid, while φ_s and λ_s are the coordinates of the shoreline. The distance between each shoreline point and the cell centroid is computed, and the minimum among all calculated distances is retained (see Fig. 1b).

$$WED = \frac{1}{2}\cdot\frac{\sum_{j=1}^{N_t}\rho_H\cdot WS_{H,j}^3\cdot\Delta t_j}{N_{years}} \quad (6)$$

$$A_{WT} = a_f\cdot A_{cell} \quad (7)$$

$$d = \frac{D_E}{2}\cdot\theta \quad (8)$$

$$\theta = 2\cdot\sin^{-1}\sqrt{\text{hav}\theta} \quad (9)$$

$$\text{hav}\theta = \frac{1 - \cos(\varphi_s - \varphi_c) + \cos\varphi_s\cdot\cos\varphi_c\cdot[1 - \cos(\lambda_s - \lambda_c)]}{2} \quad (10)$$

Cell area A_{cell} is calculated as in Eq. (11), where D_E is the Earth diameter (D_E = 12,742 km), and φ_c is the latitude of cell's centroid.

$$A_{cell} = \left(\frac{\pi}{180}\cdot\frac{D_E}{2}\cdot 1000\right)^2\cdot\Delta\varphi\cdot\Delta\lambda\cdot\frac{1}{\cos\varphi_c} \quad (11)$$

Thus, the maximum number of wind turbines N_{WT} that can be installed within each cell (see Eq. (12)) can be calculated by assuming that the occupation area A_o per one wind turbine depends on WT diameter, as per Eq. (13), by assuming a downstream spacing of 7 rotor diameters with cross-wind spacing of 5 diameters [20].

$$N_{WT} = \frac{A_{WT}}{A_o} \quad (12)$$

$$A_o = 7\,D\cdot 5\,D \quad (13)$$

Thus, if N_{WT} identical wind turbines are installed, Eq. (14) allows calculating the yearly power output per unit ground area, where P_{WT} is wind turbine power generation, which is inferred from WT power curve.

$$E_{WT,uA} = \frac{N_{WT}\cdot\sum_{j=1}^{N_t}P_{WT,j}\cdot\Delta t_j}{A_{cell}\cdot N_{years}} \quad (14)$$

3. Case study

3.1. Territory

This paper assesses the offshore wind energy potential included between latitudes from -22° to 32° and longitudes from 36° to 73°. This area includes the Mediterranean Sea, part of the Black Sea and the Atlantic Ocean, the North Sea, the Baltic Sea, and the Arctic Ocean. Figure 2 shows the seabed depth (available in [15]) and the distance from the shoreline calculated by using Eqs. (8) – (10).

In this study, *WED* is calculated across the entire offshore domain, whereas the maximum producible energy ($E_{WT,uA}$) is evaluated only in areas where wind turbine deployment is most likely, i.e., where seabed depth is lower than 200 m and the distance to the shoreline is below 200 km [17]. Areas that meet both criteria are highlighted in Fig. 3 and represent approximately 26 % of the considered offshore domain. Based on these criteria, the Baltic Sea and the North Sea are particularly suitable for the installation of offshore wind turbines. In contrast, the Arctic Ocean, the Atlantic Ocean, the Black Sea, and the Mediterranean Sea are exploitable only near the shores, as their seabed depth steeply increases, exceeding 1000 m at just approximately 100 km from the shoreline (Fig. 2a). Consequently, the waters surrounding Norway, the Iberian Peninsula, and the coasts of the Mediterranean Sea (excluding the Adriatic Sea) can be considered poorly suitable for offshore wind turbine deployment.

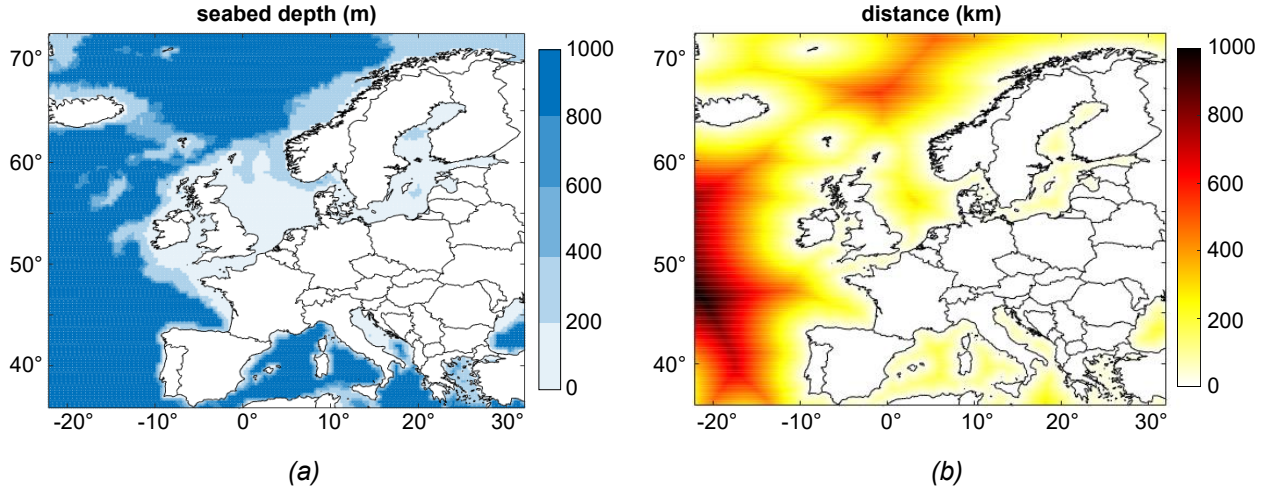

Figure 2. *a) Seabed depth [15], b) distance from the shore.*

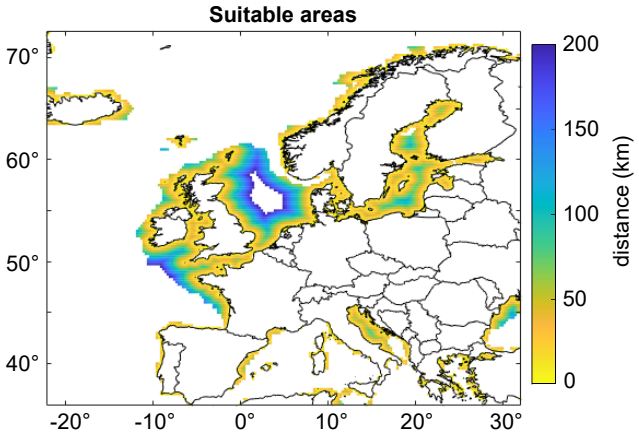

Figure 3. *Areas suitable for wind turbine deployment.*

As outlined in Eq. (7), the area effectively available for wind turbine installation (A_{WT}) is proportional to the availability factor (a_f). In this study, we consider a medium-availability scenario, in which the availability factor depends on the distance from the shore [19]. More specifically, a_f is equal to 5 % up to 10 km from the shore, 30 % between 10 and 50 km, and 60 % between 50 and 200 km from the shore. As a result, the maximum number of wind turbines that can be deployed increases with increasing distance from the shore. In this work, the availability factor is assumed to remain the same in the two considered timeframes. Thus, the number of wind turbines that can be deployed within a given cell is assumed to be constant over years.

3.2. Ambient conditions

Air temperature T (at 2 m height) and wind speed WS (at 10 m height) are extracted from CDS, which provides ambient conditions from 1951 to 2100. Ambient conditions up to year 2005 are derived by means of reanalysis, which consists of integrating historical data collected from weather stations, balloons, aircraft, and satellites with weather models to provide a consistent representation of past weather [21].

Instead, future projections are generated by using various global and regional climate models. Global climate models simulate the response of Earth's climate system to changes in greenhouse gas concentrations, regional climate models predict ambient conditions for a specific region by leveraging the outputs of the global climate model.

In this paper, ambient conditions are predicted by the regional climate model named HIRAM5 combined with the global climate model EC-EARTH, and three future scenarios (namely RCP 2.6, RCP 4.5 and RCP 8.5) are accounted for. The three RCP scenarios consider three different projected concentrations of GHG emissions. In RCP 2.6, a stringent mitigation of GHG emissions is guaranteed, RCP 4.5 is an intermediate scenario, whereas in RCP 8.5 GHG emissions will further increase in the 21st century [22, 23]. The RCP scenarios entail a different increase in the global air temperature that, in the year 2100, will be 2 °C (RCP 2.6), from 2 °C to 3 °C (RCP 4.5), or 5 °C (RCP 8.5) higher than in the preindustrial era [23].

The time granularity Δt of the ambient conditions reported in CDS is 3 hours.

3.3. Wind turbine

As outlined in Eq. (14), the total power output $E_{WT,uA}$ is proportional to the number of wind turbines N_{WT} that can be installed in each cell. In this paper, we consider the wind turbine Vestas V90-3.0 MW [16], i.e., an upwind wind turbine with a three-blade rotor, which is suitable for both onshore and offshore applications. Both rotor diameter and hub height are equal to 90 m [24]. The power curve of the considered wind turbine under standard conditions (i.e., ρ_{std} = 1.225 kg/m^3) is shown in Fig. 4. The cut-in and cut-off wind speeds are 4 m/s and 25 m/s, respectively. Power generation P_{WT} increases as wind speed increases (see Fig. 4), but P_{WT} remains constant and equal to the size of the wind turbine (3 MW) if wind speed is higher than 17 m/s.

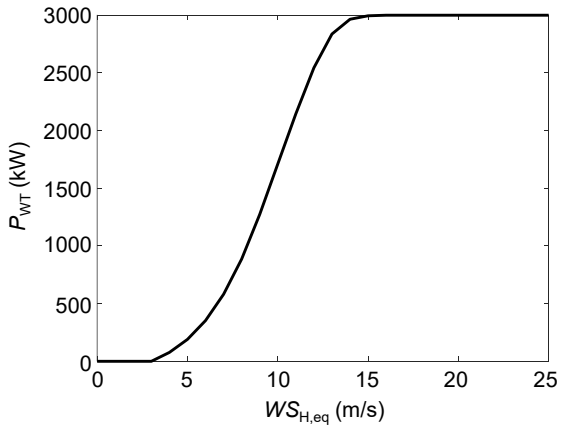

Figure 4. *Power curve of Vestas V90-3.0 MW wind turbine under* ρ_{STD} = 1.225 kg/m^3 *[24].*

The Vestas V90-3.0 MW wind turbine is pitch-regulated [24]. For this reason, for a given air density ρ_H (calculated as in Eq. (5)), Eq. (15) provides actual power generation. As a result, an increase in air temperature leads to a reduction in the equivalent wind speed ($WS_{H,eq}$), with a consequent decrease in the generated power.

$$WS_{H,eq} = WS_H \cdot \left(\frac{\rho_H}{\rho_{std}}\right)^{1/3} \quad (15)$$

In this paper, we assume that both N_{WT} and power curves do not vary over time. In such a manner, the sole influence of ambient conditions is highlighted.

3.4. Analyses

The analyses documented in this paper aim at assessing the impact of climate change on wind speed features (i.e., scale factor C, shape factor k, mean μ and mode v), wind energy density (WED) and power generation ($E_{WT,uA}$). To this purpose, such variables are calculated over two different time frames: a past time frame, used as the benchmark, which comprises the period from 2000 to 2024 (labelled as “2000”) and a future time frame ranging from 2050-2074 (labelled as “2050”). Each time frame is composed of twenty-five years, which corresponds to the economic lifetime of wind turbines [25].

Wind speed features are derived by modeling wind speed data by means of a Weibull distribution function [26, 27]. The scale factor represents the scale of the Weibull distribution: a lower value shifts the distribution to lower wind speed values. Instead, the shape factor determines the shape of the distribution; as the shape factor decreases, the maximum of the function progressively shifts toward lower wind speeds, while the frequency probability of events with high wind speed increases. The mean wind speed and the mode (i.e., the value with the highest probability) can be calculated by using Eqs. (16) and (17), respectively, and solely depend on scale and shape factors.

$$\mu = \frac{C}{k} \cdot \Gamma\left(\frac{1}{k}\right) \tag{16}$$

$$v = C \cdot \left(1 - \frac{1}{k}\right)^{\frac{1}{k}} \tag{17}$$

Instead, wind energy density and power generation are calculated as discussed in Section 2.

The impact of climate change on each variable Y is provided by its relative variation Δ over the two time frames, as per Eq. (18). Variation in wind speed features, as well as *WED*, is calculated across the entire offshore domain, whereas variation in producible energy (i.e., $E_{WT,uA}$) is evaluated only in areas where wind turbine deployment is most likely.

$$\Delta = \frac{Y_{2050} - Y_{2000}}{Y_{2000}} \tag{18}$$

4. Results

Wind energy density and wind speed, calculated over the period 2000–2024 at the hub height are shown in Figs. 5 and 6. Wind energy density (Fig. 5) mainly depends on the distance from the coast. In fact, wind features (Fig. 6) typically become more favorable for power generation, and there are no physical obstacles. In general, wind energy density rapidly increases within the first few kilometers from the coast and then tends to remain approximately constant once open sea conditions are reached.

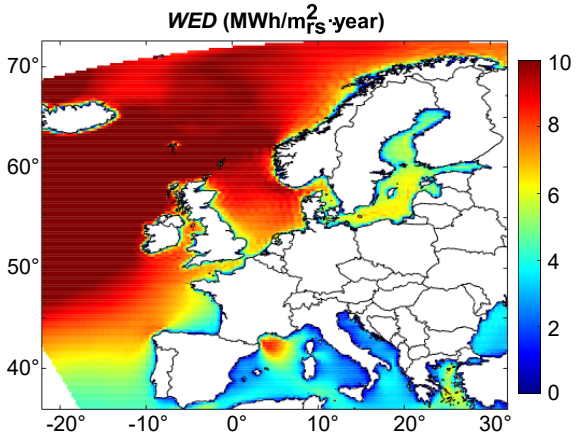

Figure 5. *Yearly wind energy density (years 2000 – 2024).*

The Atlantic Ocean, the North Sea, and the Arctic Ocean exhibit the highest wind energy density, as they are characterized by higher wind speed values and lower variability throughout the year (i.e., higher shape factor). Enclosed or semi-enclosed seas (i.e., the Mediterranean Sea, the Black Sea, and the Baltic Sea) are generally less attractive. In particular, the Mediterranean Sea typically presents the lowest *WED* due to lower values of the Weibull parameters, indicating that wind generally blows with lower intensity. The only exception is the Gulf of Lion, where wind energy density is comparable to the one in the North Sea (i.e., approximately 8 MWh/m^2_{rs}·year). Because of significant seabed depths (see Fig. 2a), floating wind farms may be a suitable option for such a location.

Figure 7a shows the number of wind turbines per unit ground area ($N_{WT,uA}$), hereafter referred as to wind turbine density, in regions where seabed depths are lower than 200 m and the distance from the coast is below 200 km. Since protected areas — which depend on geographical location — are not taken into account, three distinct zones can be identified. For a medium exploitation scenario within 10 km from the coast, wind turbine density is approximately 0.14 units/km^2, and it increases to about 1.06 units/km^2 and finally reaches 2.11 units/km^2 in areas very far from the coast.

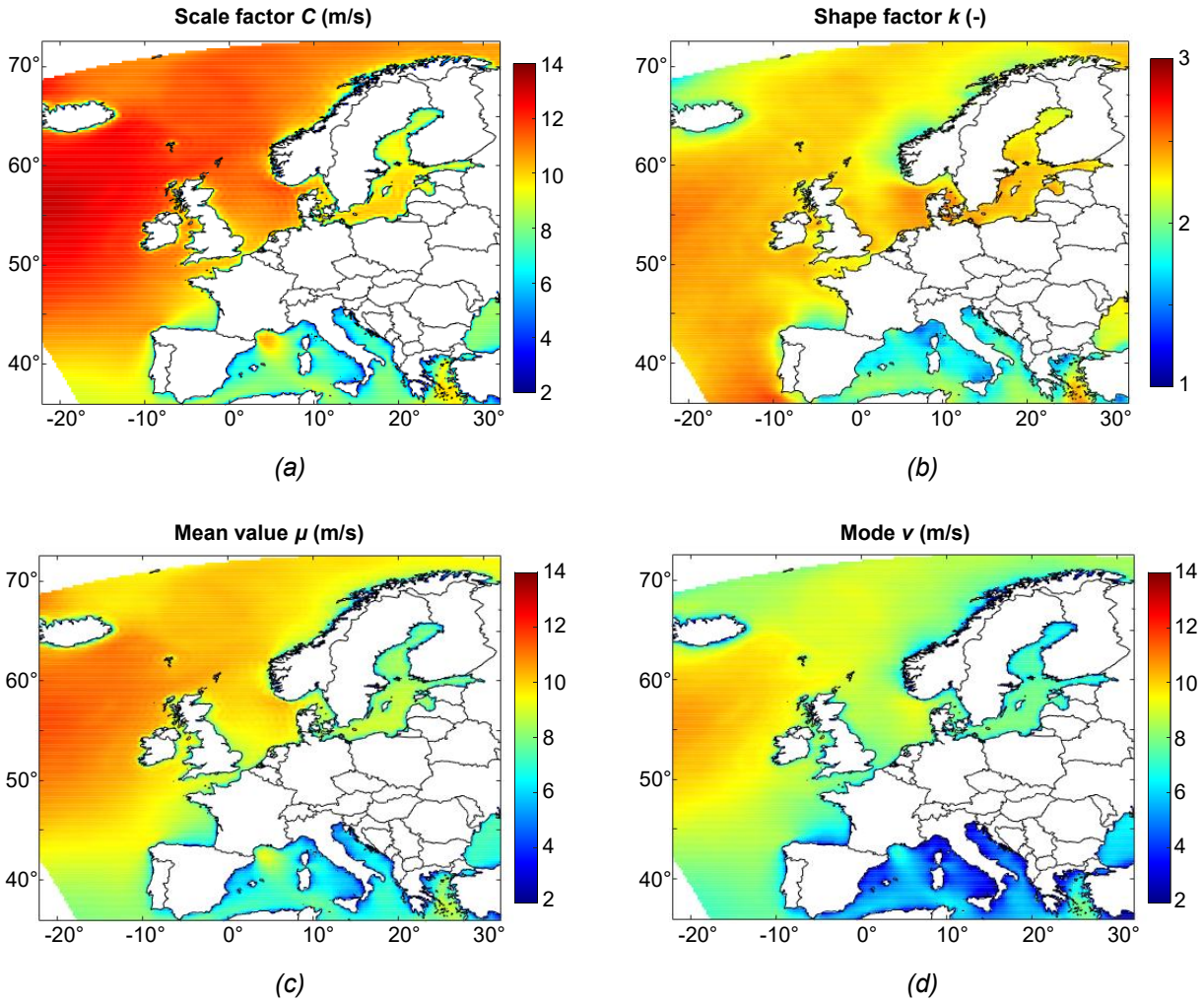

Figure 6. *a) Scale factor, b) shape factor, c) mean value, d) mode (years 2000 – 2024).*

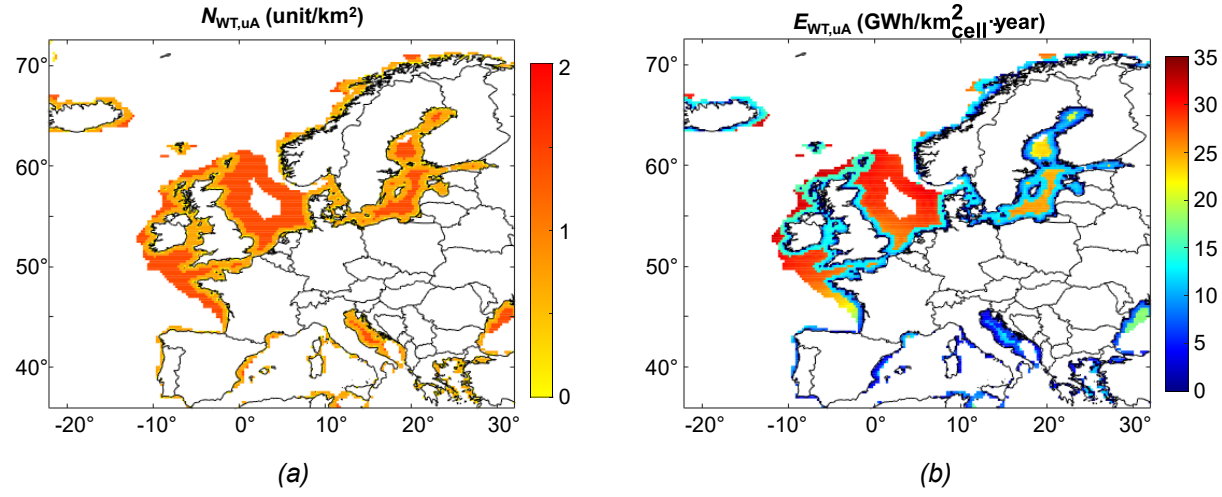

Figure 7. *a) Number of wind turbines per unit ground area, b) yearly power output per unit ground area (years 2000 – 2024).*

Figure 7b, which shows the yearly electricity production per unit ground area, confirms that the lowest power production occurs in the Mediterranean Sea, whereas the North Sea is the most attractive region. In fact, by assuming the same turbine technology and number of wind turbines deployed within a given territory, electricity production in the waters surrounding the United Kingdom (both in the North Sea and in the Atlantic Ocean) is more than twice the value expected in the Mediterranean Sea.

The combined analysis of Figs. 2a, 3, 5, 6, and 7b clearly highlights that the Atlantic Ocean and the North Sea are highly suitable areas for offshore wind energy exploitation thanks to both favorable climatic conditions and shallow seabed. This result is supported by the fact that the UK is the country with the largest installed offshore wind capacity in Europe, by accounting for more than 40 % of the total European offshore wind capacity [28]. Despite having a moderate power generation (up to approximately 26 GWh/km$^2_{cell}$·year) thanks to both favorable climatic conditions and relatively shallow seabed (Fig. 3), the Baltic Sea is currently only marginally exploited. For example, the installed offshore wind capacity in Sweden and Finland represents only about 0.5 % and 0.3 %, respectively, of the total European capacity [28].

Conversely, the potential of the waters surrounding Italy, Spain, and Portugal is currently extremely limited due to both the very large seabed depths reached even a few kilometers from the shore and, particularly in the case of Italy, usually low wind speeds.

Figure 8 provides the variation in wind speed features and wind energy density in the period 2050 – 2074 compared to the reference period (2000 – 2024). The whiskers extend to the most extreme variations that are not considered outliers, while outliers are represented by red crosses. The red horizontal line indicates the median variation, whereas the blue box delimits the interquartile range (from the 25th to the 75th percentile).

The variation in wind speed features remains relatively limited, generally ranging between ±5 % in all scenarios. In contrast, *WED* exhibits larger variations (usually between ±10 %) for two main reasons. First, *WED* depends on the cube of wind speed; therefore, small variations in wind speed are magnified. Second, *WED* is also proportional to air density, which is expected to vary because of temperature increase up to 5 °C (for RCP 8.5). As can be grasped from Fig. 8, the considered RCP scenario mainly affects outliers, and the expected variation for each physical quantity becomes progressively more pronounced moving from RCP 2.6 to RCP 8.5.

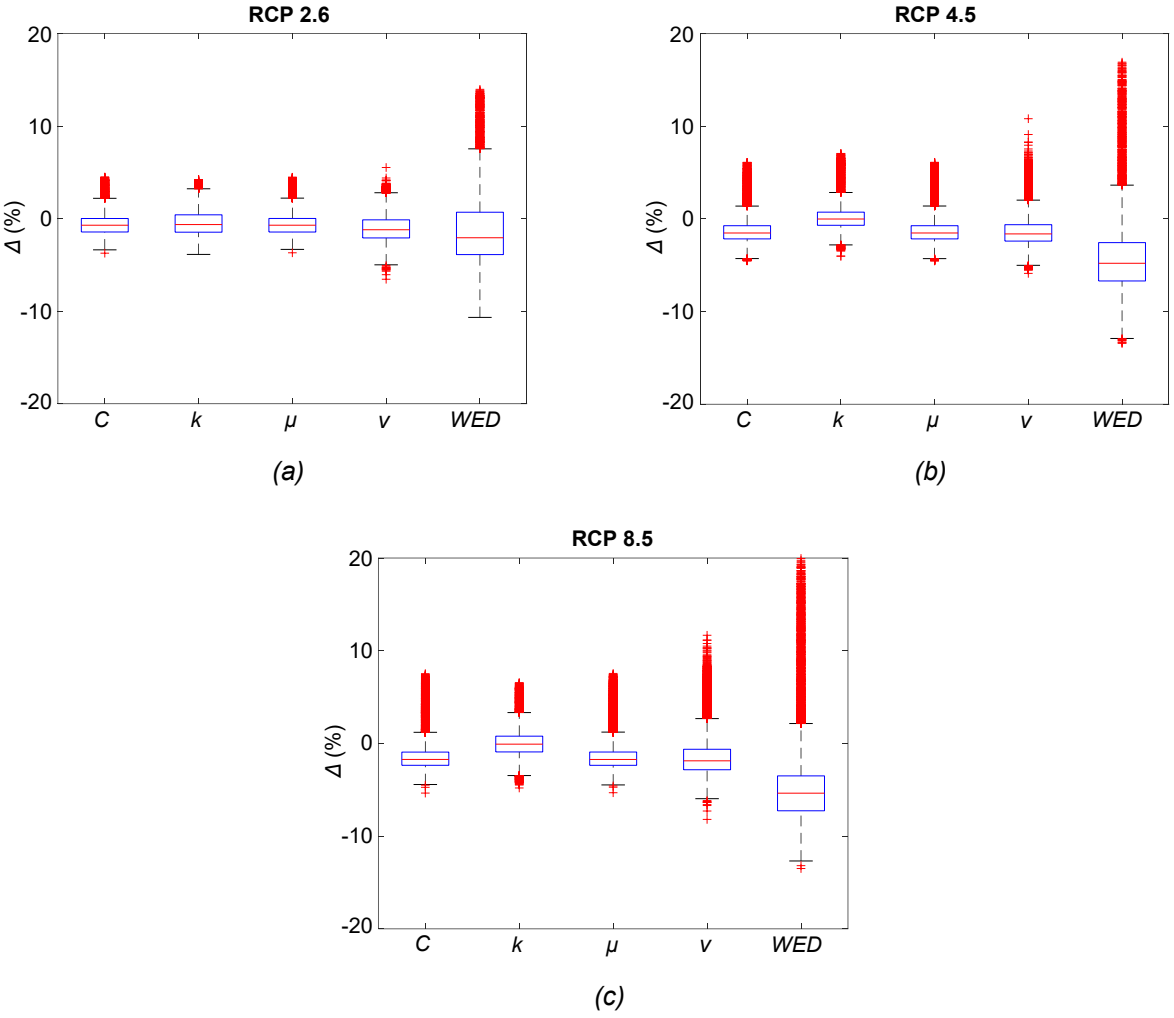

Figure 8. *Relative variation in wind speed characteristics and WED: a) RCP 2.6, b) RCP 4.5, c) RCP 8.5.*

The European wind energy density may decrease on average from −1.6 % under RCP 2.6 to −4.7 % under RCP 8.5, suggesting that the overall impact of climate change may be relatively limited. However, stronger local variations are expected. For instance, in the Arctic Ocean, wind energy density may increase by up to

20 %, as also reported in [5]. The areas most affected by *WED* reductions include the Danish coast, where values may decrease by approximately 10 %, as well as some regions of the Atlantic Ocean, both offshore and near the Irish coast. However, these latter areas are characterized by very large seabed depths (up to about 1000 m), making their exploitation particularly challenging. Despite this decrease, these areas will still have the highest wind energy density.

Similar considerations apply to the variation in electricity production in areas with seabed depths lower than 200 m and distances from the coast below 200 km (Fig. 9). Overall, a decrease in electricity production is observed, and this effect becomes more pronounced when moving from the RCP 2.6 to the RCP 8.5 scenario. European power generation may decrease on average from 0.7 % under RCP 2.6 to 3.4 % under RCP 8.5. However, more pronounced local variations are expected, particularly near the Portuguese coast and in the English Channel, where reductions of approximately −10 % are projected. All other areas show more limited changes, ranging between −5 % and +5 %.

The variation in both *WED* and electricity production depends on two main physical variables, i.e., wind speed and air temperature, but the dominant effect is determined by variations in wind speed, while the increase in air temperature has a lower influence on *WED* and electricity production [29].

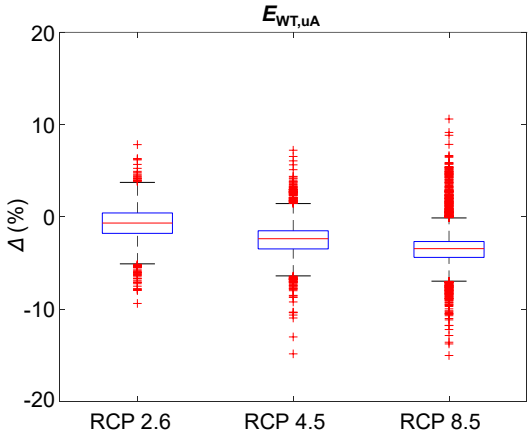

Figure 9. *Relative variation in yearly power output.*

In conclusion, the results of this study are consistent with the findings reported in [5], indicating a projected decrease in offshore wind energy potential in Europe.

By combining the results of this study with the findings reported in a previous study by the same authors [29], it is possible to derive some general guidelines for the future of both offshore and onshore wind energy in Europe (see Fig. 10).

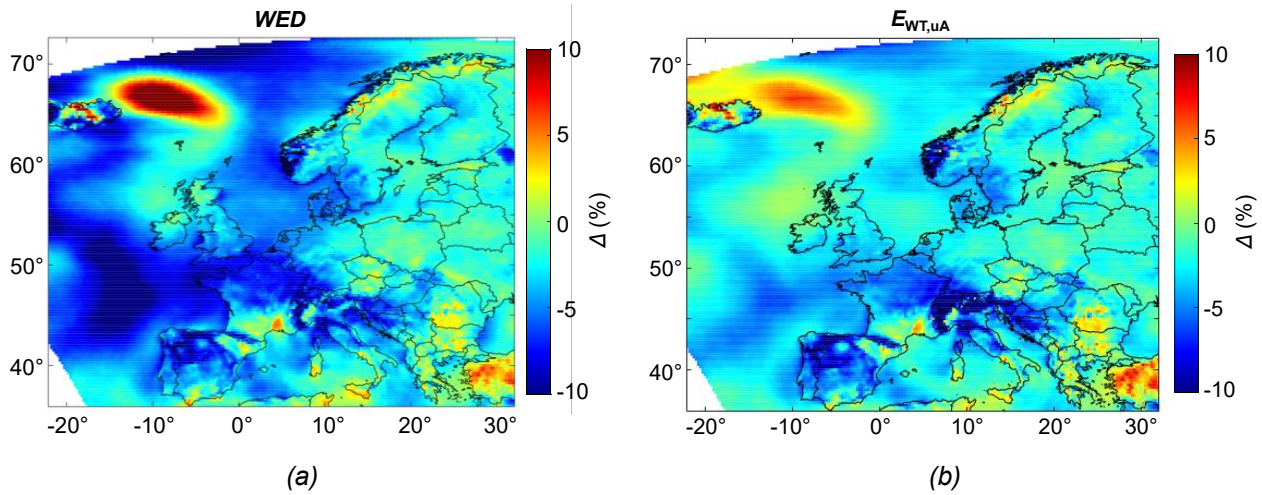

Figure 10. *Variation in: a) wind energy density, b) power output (onshore and offshore areas, RCP 4.5).*

In both cases, an overall decrease in wind energy density and power output is likely to occur. Consequently, the overall attractiveness of wind energy in Europe may gradually decline in the next decades, despite its key role in the energy transition. The largest declines are projected in regions with the highest potential (e.g., the Atlantic Ocean and the North Sea, as well as France, Germany, and Denmark). By contrast, the attractiveness

of wind energy in eastern areas (e.g., Baltic Sea, Baltic countries, Ukraine) may decrease more gradually, likely due to their greater distance from open seas (Fig. 10).
Moreover, the impact of climate change on both onshore and offshore wind energy is generally comparable in magnitude, except in certain mountainous areas (e.g., Alps), where producible power may decrease by more than 40 %, but wind energy production is relatively small.
Finally, variations in wind energy density are typically larger than those observed in energy production. In fact, power output depends on both air density and wind speed through the power curve of the wind turbine.

5. Conclusions

This paper assessed the impact of climate change on the potential of offshore wind energy in Europe. Wind energy potential was evaluated by developing a methodology that allowed calculating both wind energy density (*WED*) and power generated by a wind farm based on ambient conditions (i.e., wind speed and air temperature) and wind turbine characteristics (i.e., power curve, rotor diameter, hub height, and control strategy). The developed methodology was applied to the European region, including the Mediterranean Sea, the North Sea, the Baltic Sea, parts of the Black Sea, the Atlantic Ocean, and the Arctic Ocean.

Wind energy density and power generation were assessed for two time frames, i.e., 2000–2024 and 2050–2074. Future projections were analyzed under three different scenarios (i.e., RCP 2.6, RCP 4.5, and RCP 8.5), which differ in greenhouse gas emission concentrations.

At present, the Atlantic Ocean and the North Sea proved to be highly suitable areas for offshore wind energy exploitation, as they exhibited the highest *WED* and power generation, combined with shallow seabed depths. In contrast, enclosed or semi-enclosed seas (i.e., the Mediterranean Sea, the Black Sea, and the Baltic Sea) generally showed lower attractiveness. For instance, power generation in areas surrounding the United Kingdom could be more than twice the value observed in the Mediterranean Sea.

Due to climate change, variations in *WED* were typically within ±10 %, with the exception of localized areas (e.g., Arctic Ocean), where larger changes were expected. In contrast, variations in power generation were generally smaller.

In conclusion, the potential of offshore wind energy may decrease in the coming decades, particularly in areas that are currently the most attractive. These findings may be helpful for policy makers, given the key role of wind energy for energy transition.

Nomenclature

a_f	availability factor, %
A_{cell}	cell area, m^2
A_o	occupation area, km^2/unit
A_{WT}	area for wind turbine installation, m^2
C	scale factor, m/s
d	distance, km
D	rotor diameter, m
D_E	Earth diameter, km
$E_{WT,uA}$	yearly power output per unit ground area, $kWh/m^2 \cdot year$
g	gravitational acceleration, m/s^2
GHG	greenhouse gas
H	hub height, m
k	shape factor, -
N_t	number of time stamps, -
N_{WT}	number of wind turbine, -
$N_{WT,uA}$	number of wind turbine per unit ground area, $unit/km^2$
N_{years}	number of years, -
p_H	pressure at hub height, Pa
P_{WT}	power output, kW
R	gas constant, J/kg·K
Δt	time granularity, h
T_H	temperature at 10 m height, °C
$T_{2\,m}$	temperature at 2 m height, °C
WED	yearly wind energy density (per unit rotor swept area), $Wh/m^2_{rs} \cdot year$

WS_H wind speed at hub height, m/s

$WS_{H,eq}$ equivalent wind speed at hub height, m/s

$WS_{10\ m}$ wind speed at 10 m height, m/s

WT wind turbine

Y variable

z surface roughness, m

Greek symbols

α Hellman exponent, -

γ temperature coefficient, °C/m

Γ gamma function

Δ variation, -

θ central angle, -

$\Delta\lambda$ spatial resolution (longitude), °

λ_c longitude of cell centroid, °

λ_s longitude of shoreline, °

μ mean wind speed, m/s

v mode, m/s

ρ_H air density at hub height, kg/m^3

ρ_{std} air density under standard conditions, kg/m^3

$\Delta\varphi$ spatial resolution (latitude), °

φ_c latitude of the cell centroid, °

φ_s latitude of shoreline, °

References

[1] IPCC, 2013: Climate change 2013: the physical science basis, Contribution of Working Group I to the Fifth Assessment Report of the Intergovernmental Panel on Climate Change, Cambridge University Press, Cambridge, United Kingdom and New York, NY, USA, 2013.

[2] IEA, 2022, World Energy Outlook 2022.

[3] Chen, Y., Yue, X., Tian, C., Letu, H., Wang, L., Zhou, H., Zhao, Y., Fu, W., Zhao, X., Peng, D., Zhang, J., 2023, Assessment of solar energy potential in China using an ensemble of photovoltaic power models, Science of the Total Environment, 877, 162979.

[4] Jiang, H., Lu, N., Yao, L., Qin, J., Liu, T., 2023, Impact of climate changes on the stability of solar energy: Evidence from observations and reanalysis, Renewable Energy, 208, 726-736.

[5] Warder, S.C., Piggott, M.D., 2025, Mapping global offshore wind wake losses, layout optimisation potential, and climate change effects, Energy, 331, 136573.

[6] Martinez, A., Murphy, L., Iglesias, G., Evolution of offshore wind resources in Northern Europe under climate change, 2023, Energy, 269, 126655.

[7] Thomas, B., Costoya, X., deCastro, M., Iglesias, G., Gomez-Gesteira, M., 2026, Forecasting offshore wind energy in Atlantic Europe using CMIP6 dynamically downscaled data, Energy, 342, 139595.

[8] Nagababu, G., Patwa, P., Puppala, H., Singh Kachhwaha, S., Sricharan, V.V.S., Prasad, K.M.V.V., Arun Kumar, S.V.V., Sharma, R., 2026, Refining offshore wind energy potential estimates through the integration of technological evolution and climate change projections, Energy, 342, 139673.

[9] Meucci, A., Grossmann-Matheson, G., Su, C.H., Hally, B., Hernaman, V., Machado, D.A., Tamizi, A., Young, I.R., 2026, Resilience of offshore wind resources in Australia under climate change using CMIP6 CORDEX projections, Energy and Climate Change, 7, 100236.

[10] Martinez, A., Iglesias, G., 2024, Global wind energy resources decline under climate change, Energy, 288, 129765.

[11] Ji, L., Li, J., Sun, L., Wang, S., Guo, J., Xie, Y., Wang, X., 2024, China's onshore wind energy potential in the context of climate change, Renewable and Sustainable Energy Reviews, 203, 114778.

[12] Manservigi, L., Losi, E., Gonzalez-Salazar, M., Castorino, G.A.M., Spina, P.R., Venturini, M., 2024, Impact of climate change on solar PV potential in Europe, Proceeding of 37th International Conference on Efficiency, Cost, Optimization, Simulation and Environmental Impact of Energy Systems (ECOS 2024), pp. 593-604, 30 June - 5 July 2024, Rhodes, Greece.

[13] Russo, M.A., Carvalho, D., Martins, N., Monteiro, A., 2022, Forecasting the inevitable: A review on the impacts of climate change on renewable energy resources, Sustainable Energy Technologies and Assessments, 52, 102283.

[14] Martinez, A., Iglesias, G., 2024, Climate change and wind energy potential in South America, Science of the Total Environment, 957, 177675.

[15] Copernicus Climate Data Store (CDS). Available: https://cds.climate.copernicus.eu/#!/home. (Accessed on 10th March 2026).

[16] Gonzalez-Salazar, M., Poganietz, W.R., Evaluating the complementarity of solar, wind and hydropower to mitigate the impact of El Nino Southern Oscillation in Latin America, Renewable Energy 174 (2021) 453-467.

[17] Satymov, R., Bogdanov, D., Breyer, C., 2025, Techno-economics of offshore wind power in global resolution, Applied Energy 393 125980.

[18] Federal Office of Meteorology and Climatology MeteoSwiss, https://www.meteoswiss.admin.ch/weather/weather-and-climate-from-a-to/temperature/decreases-in-temperature-with-altitude.html.

[19] Deng, Y.Y., Haigh, M., Pouwels, W., Ramaekers, L., Brandsma, R., Schimschar, S., Grozinger, J., de Jager, D., 2015, Quantifying a realistic, worldwide wind and solar electricity supply, Global Environmental Change 31, 239-252.

[20] Lu, X., McElroy, M.B., Kiviluoma, J., 2009, Global potential for wind-generated electricity, PNAS, 106, 10933-10938.

[21] Bartók, B., Tobin, I., Vautard, R., Vrac, M., Jin, X., Levavasseur G., Denvil S., Dubus L., Parey S., Michelangeli P.A., Troccoli, A., Saint-Drenan, Y.M., 2019, A climate projection dataset tailored for the European energy sector, Climate Services, 16, 100138.

[22] IPCC, 2007: Summary for Policymakers. In: Climate Change 2007: The Physical Science Basis. Contribution of Working Group I to the Fourth Assessment Report of the Intergovernmental Panel on Climate Change, Cambridge University Press, Cambridge, United Kingdom and New York, NY, USA.

[23] IPCC, 2014: Climate Change 2014: Synthesis Report. Contribution of Working Groups I, II and III to the Fifth Assessment Report of the Intergovernmental Panel on Climate Change, Geneva, Switzerland.

[24] Vestas Wind Systems A/S, General Specification V90 – 3.0 MW, https://www.nhsec.nh.gov/projects/2008-04/documents/app_appendix_7.pdf (Accessed on 10th March 2026).

[25] IRENA, Renewable Power Generation Costs in 2022.

[26] Battisti, L., 2022, Gli impianti eolici. Città Studi Edizioni. [in italian]

[27] Wang, W., Gao, Y., Ikegaya, N., 2025, Approximating wind speed probability distributions around a building by mixture weibull distribution with the methods of moments and L-moments, Journal of Wind Engineering & Industrial Aerodynamics, 257, 106001.

[28] IRENA, Renewable energy statistics 2024.

[29] Manservigi, L., Castorino, G.A.M., Spina, P.R., Venturini, M., 2025, Impact of climate change: challenges and opportunities for onshore wind energy in Europe, Proceeding of 38th International Conference on Efficiency, Cost, Optimization, Simulation and Environmental Impact of Energy Systems (ECOS 2025), Paper ID: 7208, 29 June - 4 July 2025, Paris, France.